Switching ionic diode states with proton binding into intrinsically microporous polyamine films (PIM-EA-TB) immersed in ethanol

Journal of Electroanalytical Chemistry 922 (2022) 116751

Contents lists available at ScienceDirect

Journal of Electroanalytical Chemistry

journal homepage: www.elsevier.com/locate/jelechem

Switching ionic diode states with proton binding into intrinsically microporous polyamine films (PIM-EA-TB) immersed in ethanol

Zhongkai Li [a], Philip J. Fletcher [b], Mariolino Carta [c], Neil B. McKeown [d], Frank Marken [a,*]

[a] Department of Chemistry, University of Bath, Claverton Down, Bath BA2 7AY, UK
[b] University of Bath, Materials and Chemical Characterisation Facility, MC^2, Bath BA2 7AY, UK
[c] Department of Chemistry, Swansea University, College of Science, Grove Building, Singleton Park, Swansea SA2 8PP, UK
[d] EaStChem School of Chemistry, University of Edinburgh, Edinburgh, EH9 3FJ, UK

ARTICLE INFO

Keywords:
Ionics
Membrane
Solvent
Ion transport
Rectification
Electroosmosis

ABSTRACT

Intrinsically microporous polyamines (PIM-EA-TB) provide tertiary amine binding sites for protons and in this way allow switching/gating from a low ionic conductivity state to semipermeable anion conductivity through micropores. In ethanolic $NaClO_4$ media ionic conductivity in PIM-EA-TB films (approx. 10 μm thick; deposited asymmetrically onto a 10 μm diameter microhole in 5 μm thick Teflon) is lowered by ion exclusion compared to conductivity observed in aqueous environments. However, in the presence of protons in ethanol PIM-EA-TB films are shown to switch from essentially insulating to anionic diode behaviour. Similar observations are reported for Cu^{2+} but not for other types of cations such as Na^+, K^+, Mg^{2+} (all as perchlorate salts). Binding constants are evaluated, and protonation is identified to cause gating for both H^+ and Cu^{2+}. Both chemical and electrochemical gating/switching is demonstrated by placing a platinum electrode close to the PIM-EA-TB film and applying positive or negative bias to locally generate acid/base.

1. Introduction

Ionic diode phenomena are often associated with electrolyte transport in asymmetric nanopore and nanochannel systems [1–4], but are also commonly found for asymmetric microscale devices [5] including ionomer-coated microholes [5]. Generally, the ionic diode effect is linked to an applied bias potential triggering an asymmetric change in impedance linked, for example, to the distribution of charges. The observation of rectified ion transport has been linked to the associated rectified electroosmotic transport of water solvent molecules [6,7] and other small guest molecules such as caffeic acid [8]. Most studies to date have addressed behaviour of ionic diodes in aqueous media with applications for example in desalination [9,10], in energy conversion [11], or in sensing [12–14]. Current gating, for example with applied potentials or with ionic species, has been reported in nanopores and in nanochannels [15,16]. Recently, the effects of organic solvent environments on ion transport and on ionic diode effects in nanopores has been investigated for track-etch membranes [17]. Although aqueous media represent the obvious choice for applications of ionic rectifiers, there are interesting phenomena linked to ionic diode systems also in organic solvent systems. In this report the properties of intrinsically microporous PIM-EA-TB based ionic diodes [18] (PIM = polymer of intrinsic microporosity; EA = ethanoanthracene; TB = Tröger base; see molecular structure in Fig. 1) are investigated for chemical/electrochemical gating in ethanol environments.

Polymers of intrinsic microporosity (or PIMs [19,20]) can be employed in ionic rectifiers when charges are attached to the backbone of the polymer to create semipermeability and ion conducting channels. For PIM-EA-TB [21] the typical pore size is 1 nm and tertiary amine sites in the molecularly rigid structure have been shown to undergo protonation at approx. pH 4 in aqueous media [22]. The protonated PIM-EA-TB acts as a rigid and porous anion conductor. An asymmetric film deposit on a substrate with microhole leads to anionic diode characteristics [23]. Fig. 1A illustrates the four-electrode measurement system and Fig. 1B explains the phenomenon of electrolyte depletion (closed state) and accumulation (open state) that are responsible for a change in resistivity when changing the polarity of the applied voltage [24]. Anionic diodes are open with negative applied bias as long as the PIM-EA-TB film deposit faces the working electrode (Fig. 1A).

There is now considerable interest in ionic transport in PIM membranes [25] (even if these materials have originally been conceived for gas phase applications [26]). For applications of PIMs in redox flow cells [27] and in batteries [28] ion transport and organic solvents

* Corresponding author.
E-mail address: f.marken@bath.ac.uk (F. Marken).

https://doi.org/10.1016/j.jelechem.2022.116751
Received 31 May 2022; Received in revised form 26 July 2022; Accepted 25 August 2022
Available online 29 August 2022

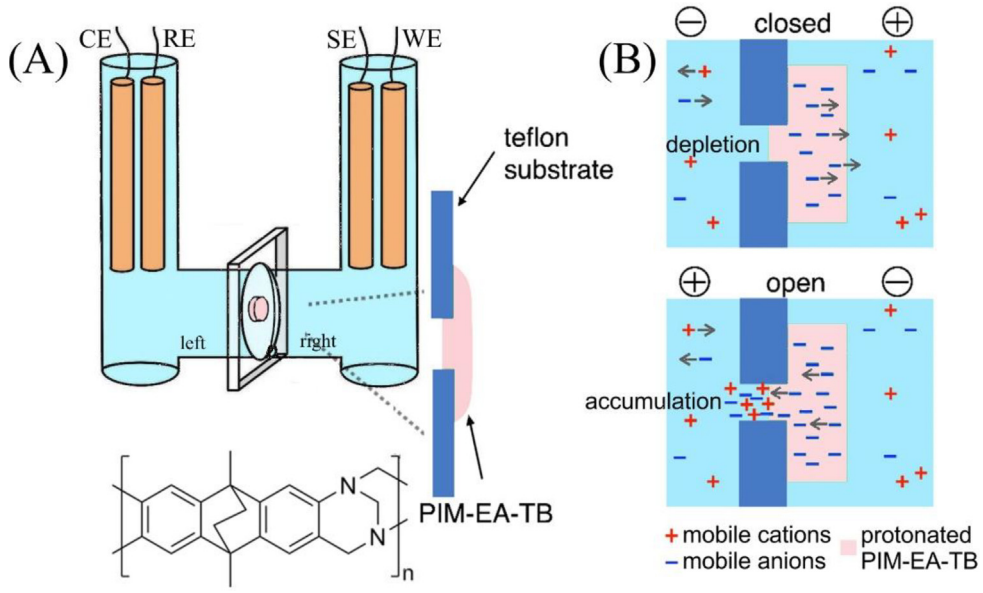

Fig. 1. (A) Four-electrode measurement configuration with PIM-EA-TB-coated microhole substrate. (B) Illustration of the mechanism resulting in electrolyte depletion and accumulation in anionic diodes.

are crucial. Here, PIM-EA-TB is investigated in ethanolic electrolyte media. In contrast to previous observations in aqueous media, the less polar ethanolic environment causes a more dramatic switching from ionic insulator to ionic diode due to protonation of PIM-EA-TB. The behaviour of $HClO_4$, $LiClO_4$, $NaClO_4$, $Mg(ClO_4)_2$, and $Cu(ClO_4)_2$ are reported and shown to be dominated by protonation effects.

2. Experimental

2.1. Reagents

The polymer PIM-EA-TB was synthesised with approx. 70 K_D molecular weight following a literature method [21]. $NaClO_4$ (≥98.0 %), $LiClO_4$ (≥95.0 %) and chloroform were purchased from Sigma-Aldrich. $HClO_4$ (ACS reagent) was purchased from Honeywell. $Mg(ClO_4)_2$ (≥80 %) was purchased from BDH Limited. $Cu(ClO_4)_2$ (98 %) was purchased from Thermo Scientific. Agarose powder was purchased from Melford ltd. All chemicals were utilised as received without further purification. Ethanol (EtOH) solutions were prepared with absolute ethanol from VWR Chemicals BDH (99.97 %). Aqueous solutions were prepared with filtered ultra-pure water (resistivity ≥ 18.2 MΩ cm at 20 ℃) from a Thermo Scientific water purification system.

2.2. Instrumentation

Electrochemical measurements were performed on a program-controlled potentiostat (Metrohm ltd Autolab PGSTAT30) for cyclic voltammetry and chronoamperometry or a Solartron Analytical ModuLab XM MTS system for electrochemical impedance spectroscopy, either in a four-electrode configuration (working, sense, counter, and reference electrodes, Fig. 2A), or in a five-electrode configuration (with a secondary working electrode, Fig. 2B). The electrochemical cell was constructed with two cylindrical cells separated by a Teflon substrate (5 μm thick). The substrate was laser-drilled with a microhole of 10 μm diameter (Laser Micromachining ltd, UK) and asymmetrically coated with a PIM-EA-TB membrane. Carbon rods (1 mm diameter) were applied as working and counter electrodes, and silver wires (0.5 mm diameter) served as quasi-sense and quasi-reference electrodes. A 3 mm platinum disk electrode (BASi Research Products, UK) was used as the secondary working electrode. Scanning electron microscopy and energy-dispersive X-ray spectroscopy were performed on a Hitachi SU390 with attached Oxford Instruments Ultim Max 170 mm^2 EDX detector.

2.3. Procedure: Preparing PIM-EA-TB films on Teflon Substrates

A laser-drilled Teflon substrate (5 μm thick. Laser Machining ltd, UK) was placed onto a glass substrate coated with a thin layer of 1 % wt. agarose gel (to prevent the coating solution from penetrating through the microhole [29]). A volume of 10 μL of 3 mg/mL solution of PIM-EA-TB in chloroform was drop-casted onto one side of the substrate. After evaporation, a uniform membrane coating was formed over the microhole region, with a thickness estimated to be typically 10 ± 5 μm [23]. The Teflon substrate was then assembled between two flanges into an electrochemical cell (Fig. 2).

3. Results and discussion

3.1. PIM-EA-TB ionic transport behaviour: Water versus ethanol

Most ion transport studies with PIM-EA-TB films to date have been carried out in aqueous electrolyte media. The PIM-EA-TB film has been shown to be protonated at approx. pH 4 [22] to give an anion-conducting microporous material. PIM-EA-TB remains uncharged at neutral pH. As a result, for ionic currents to flow, individual ions or ion pairs (anions and cations) need to diffuse simultaneously into the microporous film to create appreciable ion conductivity. The effects of the solvent on the PIM-EA-TB membrane conductivity properties have not been previously assessed. Here, ionic conductivity for water and for ethanol solvents are contrasted.

Fig. 3 shows cyclic voltammetry data for a solution of 10 mM $NaClO_4$ in water (placed into both compartments left and right of the membrane) and data for 10 mM $NaClO_4$ in ethanol. In Fig. 3A data for the empty microhole are shown and in Fig. 3B data for the PIM-EA-TB deposit are shown. In the absence of PIM-EA-TB Ohmic behaviour is observed with conductivity 560 nS for aqueous 10 mM $NaClO_4$ and 187 nS for ethanolic 10 mM $NaClO_4$. In the presence of PIM-EA-TB the current–voltage curve slopes at zero current are 57 nS for water and 4 nS for ethanol, clearly indicating a substantial change in ion

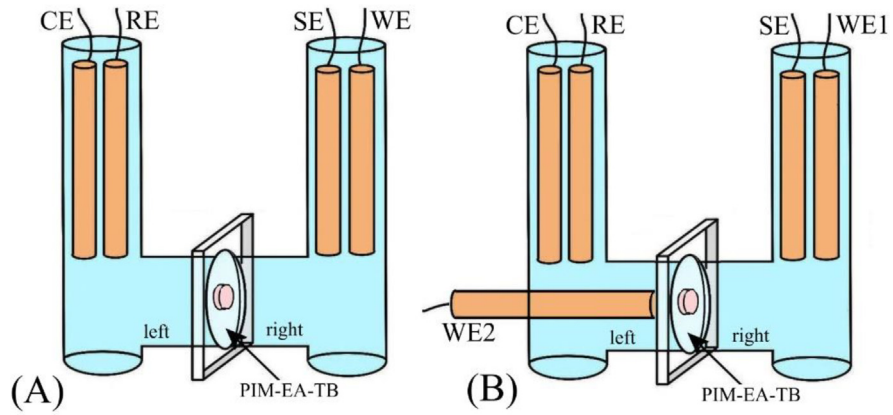

Fig. 2. (A) Illustration of the four-electrode system with working electrode (WE) and counter electrode (CE) carbon rods and reference electrode (RE) and sense electrode (SE) silver rods. (B) Five-electrode configuration with a second working electrode (a 3 mm diameter platinum disk) located close to the PIM-EA-TB membrane.

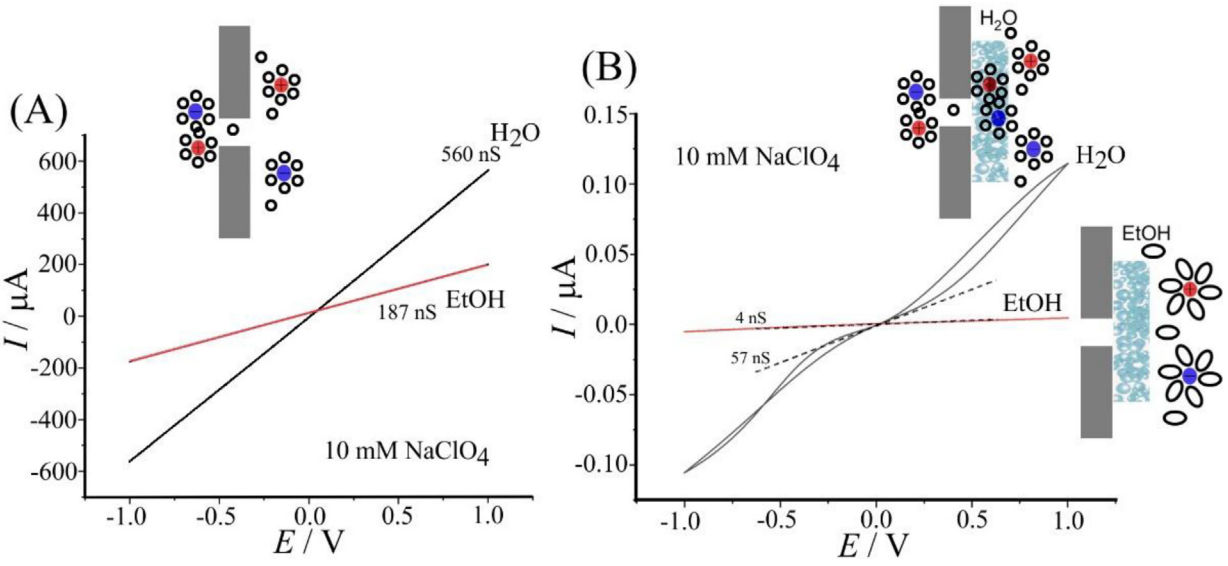

Fig. 3. Cyclic voltammograms (4-electrode configuration, scan rate 0.2 V s^{-1}) for (A) no deposit and (B) a PIM-EA-TB film deposit on 5 µm thick Teflon substrate with 10 µm diameter microhole immersed in 10 mM $NaClO_4$ in water or in ethanol. A dashed line indicates zero-current conductivity.

conductivity across the membrane when introducing PIM-EA-TB and when changing the solvent.

Generally, effects on conductivity are linked to both the solvent and the electrolyte properties. Bulk solution conductivity data (at 25 °C [30]) for $NaClO_4$ suggest that $\lambda^{\infty}_{Na^+}$ = 50.1 cm^2 S mol^{-1} in water and 20.3 cm^2 S mol^{-1} in ethanol and $\lambda^{\infty}_{ClO_4^-}$ = 67.4 cm^2 S mol^{-1} in water and 30.5 cm^2 S mol^{-1} in ethanol. This change in conductivity is associated with both changes in hydrodynamic radii and changes in viscosity. Walden's rule suggests $\lambda^{\infty}_{ion} \times \eta = constant$ with the limiting single-ion conductivity λ^{∞}_{ion} and the dynamic viscosity η. Viscosity values (at 25 °C) for water 0.89 mPa s and for ethanol 1.1 mPa s would suggest a relative decrease in conductivity in ethanol of about 20 % (taking only viscosity into account). But the limiting single ion conductivity values from literature suggest a 60 % to 55 % decrease for Na^+ and ClO_4^-, respectively. This more substantial change is therefore likely to be dominated by the solvent shell increasing the hydrodynamic diameter of ions in ethanol and/or an increased tendency towards ion pairing. The experimental value for an open microhole in Fig. 3A suggests a 66 % decrease in conductivity consistent with limiting ion conductivity data.

Both viscosity and ion conductivity cannot explain the experimental data for the PIM-EA-TB film (Fig. 3B). The experimental values for conductivity through the PIM-EA-TB coated microhole estimated at zero current as 4 nS for ethanol and 57 nS for water (see Fig. 3B) suggest a more dramatic change linked to the microporous polymer. It is possible that in ethanol the population of ions (and ion pairs) in the PIM-EA-TB remains lower probably due to size exclusion of solvated ions/ion pairs. Therefore, the ionic conductivity of PIM-EA-TB in ethanol is much lower in contrast to that in aqueous solution. Perhaps interestingly, the ion currents in water increase in a non-linear fashion with applied potential (probably due to additional ion populations getting dragged by the electric field into the microporous structure). A similar effect was not observed in ethanol (within the potential range explored here). In ethanol, PIM-EA-TB essentially behaves Ohmic and remains more insulating even with applied bias potentials. The effect of the electrolyte cation on conductivity in PIM-EA-TB will be investigated next.

3.2. PIM-EA-TB ionic diode behaviour in ethanol I.: Survey of cations

Fig. 4 shows data for cyclic voltammetry experiments conducted in 4-electrode configuration with solutions containing ClO_4^- anions and a range of different cations in ethanol. In the presence of Na^+, Li^+, and Mg^{2+} cations predominantly resistive behaviour is observed with a

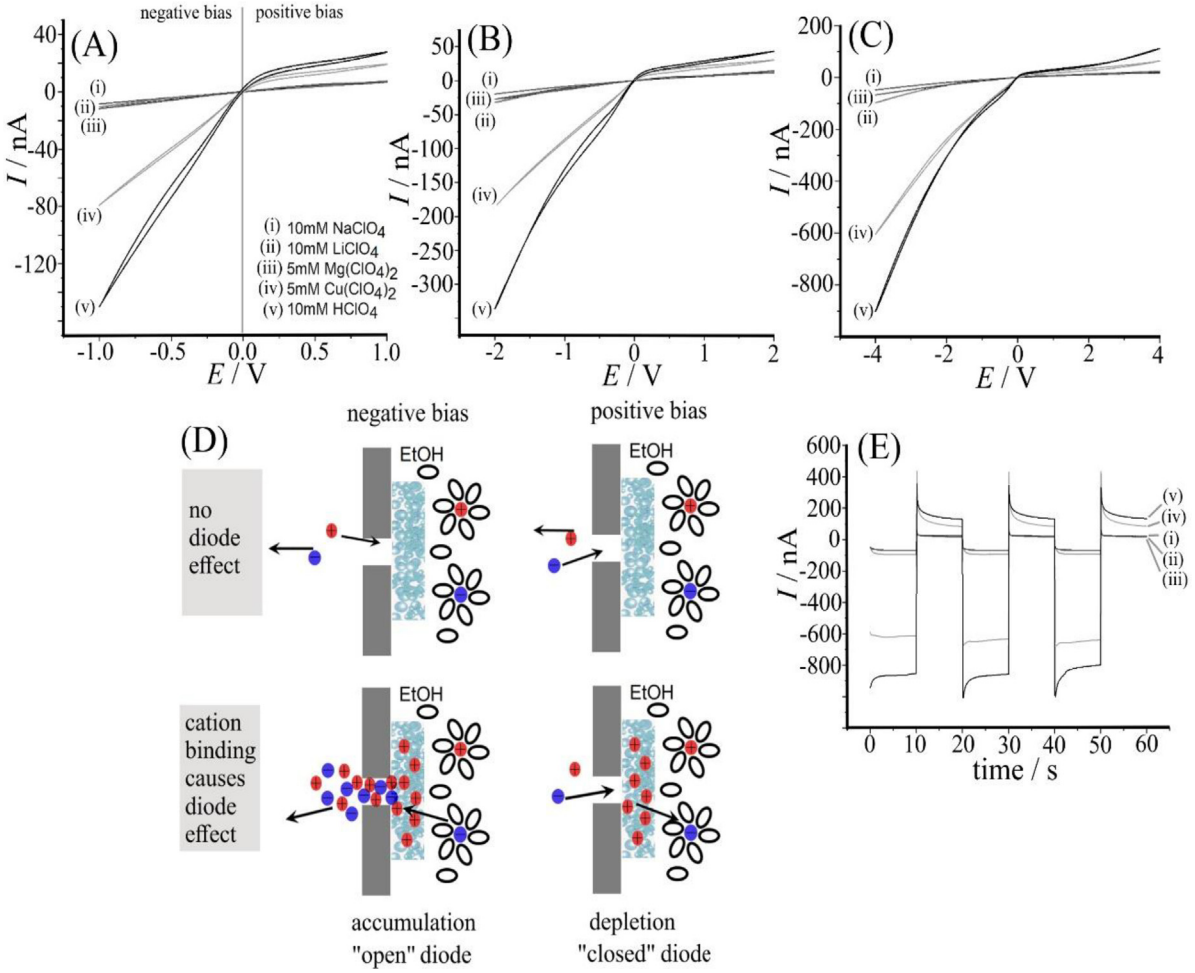

Fig. 4. Cyclic voltammograms (4-electrode configuration, scan rate 0.2 Vs^{-1}) for ethanol solutions of (i) 10 mM $NaClO_4$, (ii) 10 mM $LiClO_4$, (iii) 5 mM $Mg(ClO_4)_2$, (iv) 5 mM $Cu(ClO_4)_2$, and (v) 10 mM $HClO_4$ employing (A) a +/-1V potential window, (B) a +/-2V potential window, (C) a +/-4V potential window. (D) Illustration of ionic diode mechanism. (E) Chronoamperometry data for +/-4V potential pulses.

low rate of permeation of ions. However, for H^+ and Cu^{2+} the current–voltage curve changes characteristically with a high current at negative applied potentials and a still significant current for positive applied potentials. This asymmetry or diode effect has been explained with ion accumulation and depletion in the mircrohole region (see Fig. 1B). Similar observations are made within a potential window of +/−1 V (Fig. 4A), +/−2 V (Fig. 4B), and +/−4 V (Fig. 4C). The observed "over-voltage" of approx. 0.1 V positive or negative of 0.0 V can be understood as the voltage requirement for the concentration polarisation effect within the microhole to develop.

Both H^+ and Cu^{2+} cations seem to be able to interact with PIM-EA-TB most likely by modifying the tertiary amine functional groups in the PIM-EA-TB to give anion conducting microporous structures. A population of immobile cations in the microporous host structure is formed associated with mobile counter anions and semi-permeability due to anion transport. Anion transport under negative bias will force electrolyte into the microhole region causing a higher conductivity and the "open" diode state. In contrast, a positive bias will cause anion extraction from the microhole region or depletion (Fig. 4D).

When widening the potential window to +/−2V and +/−4V trends continue. A change in the slope of the current–voltage curve at approximately +/−2V can be attributed to over-limiting conditions and the onset of interfacial convection [31]. Chronoamperometry data (Fig. 4E) confirm the diode behaviour in the presence of H^+ and Cu^{2+} and show that the switching time for the diode is typically 2 s. The effects for H^+ and Cu^{2+} can be recognised as chemical gating whereby a chemical reagent causes the ionic diode effect to develop.

The effect of $HClO_4$ protonation of the PIM-EA-TB is expected and can be seen in qualitative energy-dispersive X-ray mapping. Fig. 5 shows data for PIM-EA-TB being seen through the microhole with both Cl and O elemental maps revealing the protonation. The same experiment for untreated PIM-EA-TB does not show Cl or O (in Fig. 6) confirming the result.

In order to further explore binding of ions to PIM-EA-TB, EDX data were obtained for a thin film of PIM-EA-TB (30 μL of 2 mg/mL PIM-EA-TB in chloroform solution drop-casted onto a Teflon substrate to give a film of approx. 2 μm thickness) exposed to ethanolic electrolyte solution (15 min in 10 mM $NaClO_4$, 10 mM $LiClO_4$, 5 mM $Mg(ClO_4)_2$, 10 mM $HClO_4$, or 5 mM $Cu(ClO_4)_2$). Samples were rinsed with pure ethanol and dried prior to EDX analysis. Data are summarised in Table 1.

From EDX data it is apparent that protonation occurs in ethanolic $HClO_4$. The presence of ClO_4^- can be linked to the detection of Cl. The Cl/N atomic % ratio is 5.3 (in pure PIM-EA-TB Cl/N is 0.0) suggesting that approx. 20 % of the nitrogen atoms in PIM-EA-TB are protonated. As expected (from voltammetric data), there is essentially no perchlorate present for samples after exposure to $NaClO_4$, $LiClO_4$, and $Mg(ClO_4)_2$. However, for $Cu(ClO_4)_2$ solution, only a trace of Cu is observed, but still the Cl/N atomic % ratio is 0.07 suggesting substantial protonation of PIM-EA-TB. Therefore, the hypothesis for Cu^{2+}

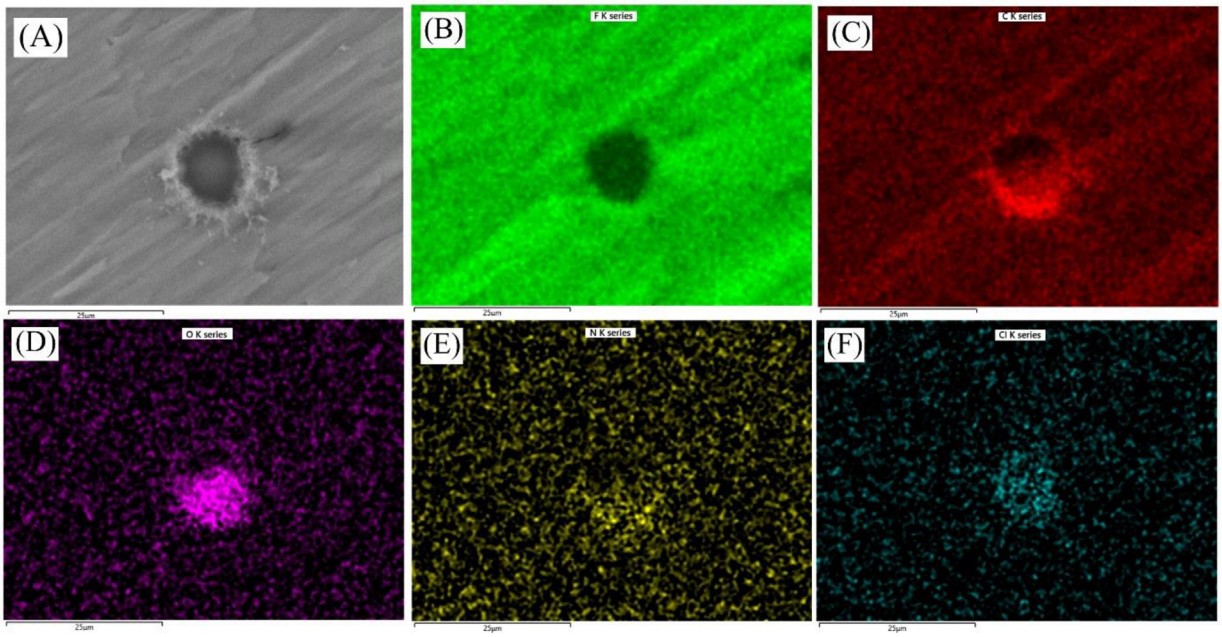

Fig. 5. Scanning electron microscopy (SEM) image of the Teflon substrate with PIM-EA-TB (with $HClO_4$ treatment) visible through the 10 μm diameter microhole. (A) SEM image and elemental maps for (B) F, (C) C, (D) O, (E) N, and (F) Cl.

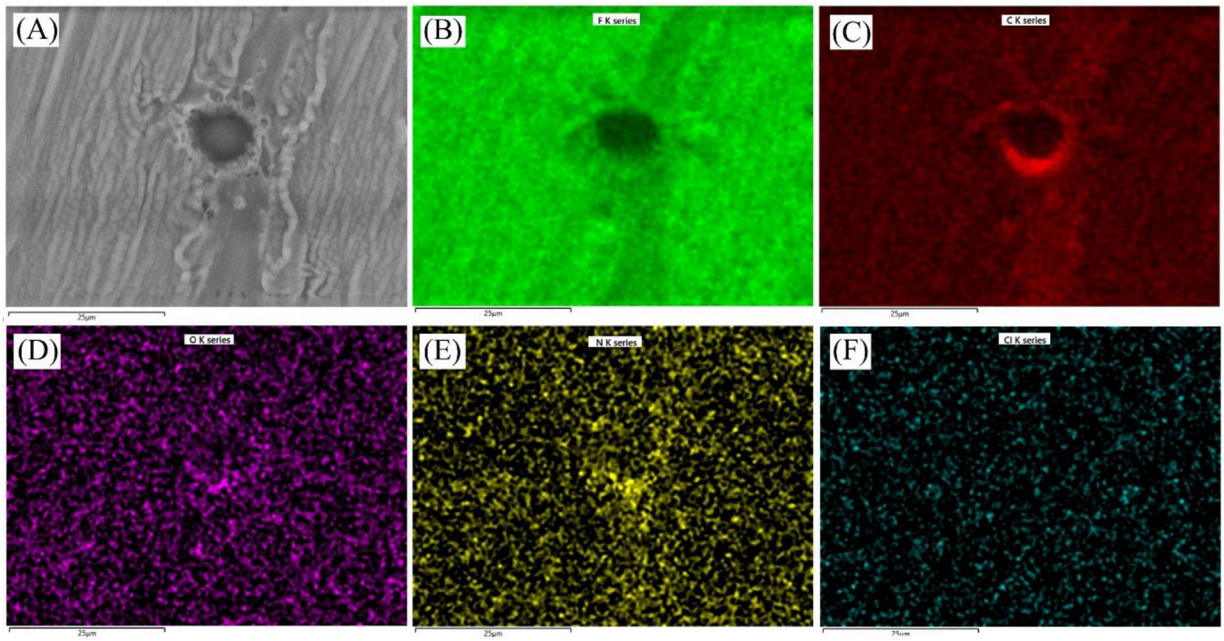

Fig. 6. Scanning electron microscopy (SEM) image of the Teflon substrate with PIM-EA-TB (without $HClO_4$ treatment) visible through the 10 μm diameter microhole. (A) SEM image and elemental maps for (B) F, (C) C, (D) O, (E) N, and (F) Cl.

reactivity in ethanol has to be based on formation of an acidic Cu^{2+} complex and protonation of PIM-EA-TB as the main mechanism for ionic diode formation. Next, the case of Cu^{2+} is investigated in more detail.

3.3. PIM-EA-TB ionic diode behaviour in ethanol II.: Chemical gating with Cu^{2+}

Data in Fig. 4 clearly show that Cu^{2+} cations are able to cause bound positive charges in the PIM-EA-TB membrane material resulting in diode-like behaviour. The availability of amine sites in the polymer backbone is likely to lead to an interactions and binding of protons (rather than direct binding of Cu^{2+}, *vide supra*). In order to explore this interaction, the effect of Cu^{2+} ethanolic concentration was investigated.

In a solution of 10 mM $NaClO_4$ the conductivity of the PIM-EA-TB film is low. When adding 5 mM $Cu(ClO_4)_2$ (on both sides), a gradual change in the cyclic voltammograms happens (over several potential cycles) associated with an increase in conductivity. Fig. 7A shows data for 20 consecutive potential cycles. The anionic diode behaviour is clearly observed but currents are only slowly increasing with time. Based on EDX data, the process responsible for this effect is PIM-EA-

Table 1
EDX data (atomic %) for PIM-EA-TB films on Teflon exposed (15 min) to 10 mM $NaClO_4$, 10 mM $LiClO_4$, 5 mM $Mg(ClO_4)_2$, 10 mM $HClO_4$, or 5 mM $Cu(ClO_4)_2$ and rinsed with ethanol prior to analysis.

Element	EtOH solution cation				
	Na^+	Li^+	Mg^{2+}	H^+	Cu^{2+}
C	63.31	54.88	64.30	55.95	68.23
N	4.82	3.24	6.78	4.61	6.05
O	0.78	0.58	1.79	6.02	3.34
F	31.06	41.26	27.06	32.54	21.88
Cl	0.01	0.01	0.07	0.87	0.41
Na	–	–	–	–	–
Mg	–	–	–	–	–
Cu	–	–	–	–	0.03
Cl/N ratio	0.002	0.003	0.01	0.19	0.07

TB protonation with the Cu^{2+} complex acting as a weak homogeneous acid in ethanol. Transport of protons into the PIM-EA-TB film appears to be slow. The dissociation of the acidic Cu^{2+} complex may be weak leading to a low proton level and therefore slow/gradual protonation of the porous polymer. The presence of further reaction intermediates (for example Cu(II) complexes permeating into the PIM-EA-TB film) cannot be ruled out.

When varying the concentration of Cu^{2+}, a pattern of reactivity correlated to Cu^{2+} concentration emerges. Fig. 7B shows that the anionic diode effect increases with Cu^{2+} concentration. Fig. 7C shows the corresponding chronoamperometry data with anionic diode effects in the presence of Cu^{2+}. Fig. 7D shows the rectification ratio (at +/−1V reaching almost 4) as a function of Cu^{2+} concentration. A switch occurs at about 10^{-4} M Cu^{2+} with a plateau (or maximum) being reached at 10^{-2} M Cu^{2+}.

In order to quantify the binding of positive charges into PIM-EA-TB, the concentration of ethanolic Cu^{2+} was varied and the zero current conductivity evaluated from cyclic voltammetry data. Fig. 7E shows the transition associated with the binding of positive charges. The data points fit a Langmuir binding isotherm with approx. $K = 2000\ (\pm 40)$ mol^{-1} dm^3 (corresponding to a concentration at half coverage of 0.5 mM Cu^{2+}). The most likely mechanism for this binding process is protonation of the tertiary amine groups in PIM-EA-TB (*vide infra*). A simple pH paper test comparing ethanolic solutions of 10 mM $NaClO_4$, $Cu(ClO_4)_2$, and $HClO_4$ suggests that there is acid in the Cu^{2+} solution (Fig. 7).

It is interesting to attempt reverting the state of the PIM-EA-TB film back to low conductivity. When changing the solution phase from 5 mM $Cu(ClO_4)_2$ in 10 mM $NaClO_4$ to pure ethanolic $NaClO_4$, the anionic diode characteristics persist, although a partial decay in diode cur-

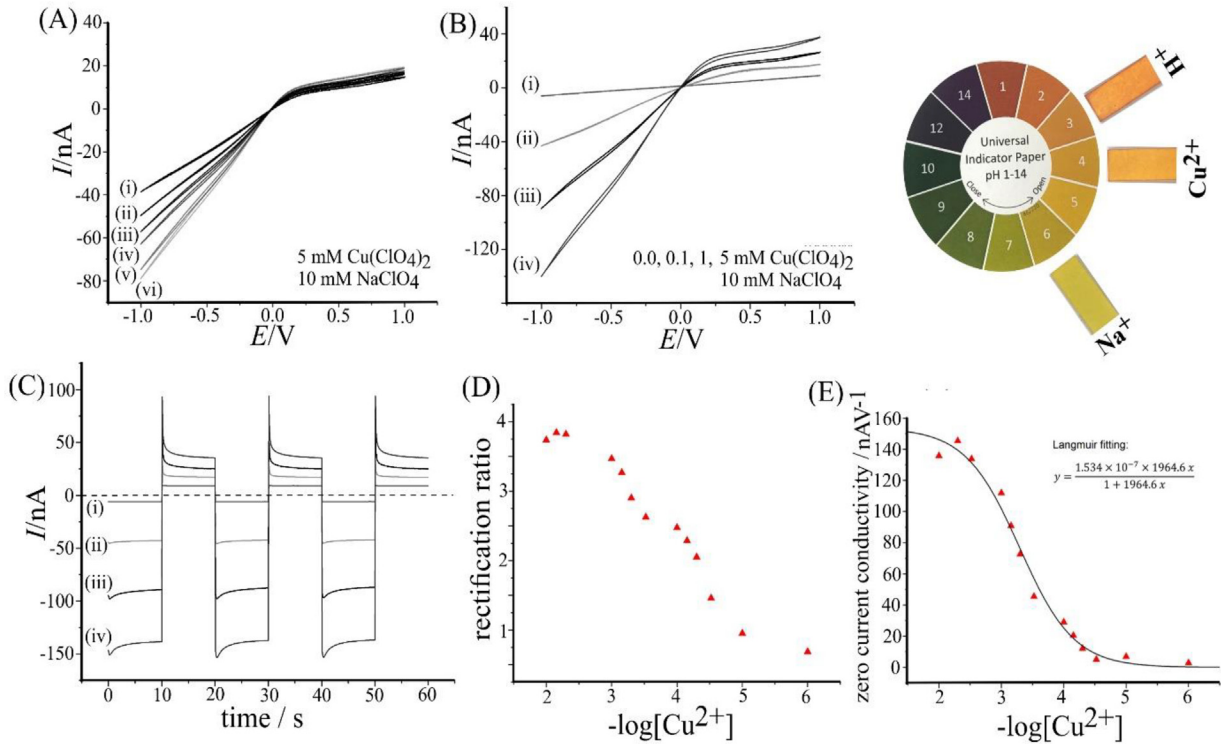

Fig. 7. (A) Cyclic voltammograms (four-electrode configuration, scan rate 0.2 Vs^{-1}) for a PIM-EA-TB membrane immersed in 5 mM $Cu(ClO_4)_2$ in ethanolic 10 mM $NaClO_4$. Potential scans 1, 4, 7, 10, 15, and 20 demonstrate the gradual development of ionic diode character. (B) Cyclic voltammograms for fully equilibrated membranes for (i) 0, (ii) 0.1, (iii) 1, and (iv) 5 mM $Cu(ClO_4)_2$ in 10 mM $NaClO_4$. (C) Chronoamperometry data (switching between −1 V and + 1 V) for (i) 0, (ii) 0.1, (iii) 1, and (iv) 5 mM $Cu(ClO_4)_2$ in 10 mM $NaClO_4$. (D) Plot of rectification ratio from chronoamperometry versus Cu^{2+} concentration. (E) Langmuir plot for zero-current conductivity (from cyclic voltammograms) versus Cu^{2+} concentration. Also shown is a photograph of pH paper colour responses to 10 mM $NaClO_4$, $Cu(ClO_4)_2$, and $HClO_4$ in ethanol.

rents is observed (not shown). The modification/protonation of the PIM-EA-TB film appears to be not reversed in the absence of Cu^{2+}. Further insight into these processes in the PIM-EA-TB will be obtained in the next section.

3.4. PIM-EA-TB ionic diode behaviour in ethanol III.: Chemical gating with protons

Proton binding into PIM-EA-TB occurs rapidly when adding $HClO_4$ into ethanolic 10 mM $NaClO_4$. Fig. 8A shows cyclic voltammograms obtained as a function of $HClO_4$ concentration. In the absence of acid (only 10 mM $NaClO_4$ present) highly insulating behaviour is observed. Then, with addition of acid (into both sides), positive and negative applied potentials cause current with asymmetry clearly revealing ionic diode behaviour (consistent with anionic diode behaviour [32]). Perhaps interestingly, when switching the solution back from 10 mM $HClO_4$ (with 10 mM $NaClO_4$) to pure 10 mM $NaClO_4$, the protonation persists. Fig. 8Aiv shows some decay of the current, but clear ionic diode behaviour persists even after 24 h. This observation is consistent with that for the Cu^{2+} case and indicative of persisting protonation in ethanolic electrolyte. In other words, in order to switch the PIM-EA-TB back into the original unprotonated state, the addition of base is required for the deprotonation.

The ionic diode effect can be expressed in terms of the rectification current ratio *I*(open diode) / *I*(closed diode). A plot of the rectification ratio in Fig. 8C based on chronoamperometry data in Fig. 6B shows a transition at approx. 1 mM $HClO_4$. In order to quantify the proton binding, a Langmuir isotherm plot is constructed based on zero current conductivity data (from cyclic voltammetry data). Fig. 9D shows a well-defined protonation process with $K = 1971\ (\pm 40)$ $mol^{-1}dm^3$ (corresponding of a concentration of half coverage of 0.51 mM H^+). This result is indistinguishable from that observed in the presence of Cu^{2+} (see Fig. 7E) and therefore strong evidence for protons to be involved in both cases. The protonation is confirmed with EDX data (see Table 2 and Fig. 8E). A mismatch of atomic % data in Fig. 8E and the zero current conductivity data in Fig. 8D can be explained with the effect of sample rinsing in pure ethanol leading to some loss and a less quantitative result for EDX.

With *chemical gating* of ionic diode behaviour demonstrated it is interesting to explore *electrochemical gating* without the need to add reagents or salts. A platinum electrode can be employed to locally produce protons (positive bias) or base (negative bias) to allow switching from insulator to ionic diode and back.

3.5. PIM-EA-TB ionic diode behaviour in ethanol IV.: Electrochemical gating with protons

Data shown in Fig. 8 represent the case of addition of $HClO_4$ on both sides of the PIM-EA-TB film. In Fig. 9 two data sets are presented for (i) addition of acid into the counter electrode compartment (left) and (ii) addition of acid into the working electrode compartment (right). With the PIM-EA-TB film being located on the working electrode side (right), the effects introduced by the acid are very different to those on the counter electrode side. On the working electrode side, even with 7 mM $HClO_4$, the diode effect is not obvious and there is evidence for hysteresis in the data suggesting that the level of protonation may change upon cycling the potential (Fig. 9E). In contrast, with $HClO_4$ addition into the counter electrode compartment, well-defined

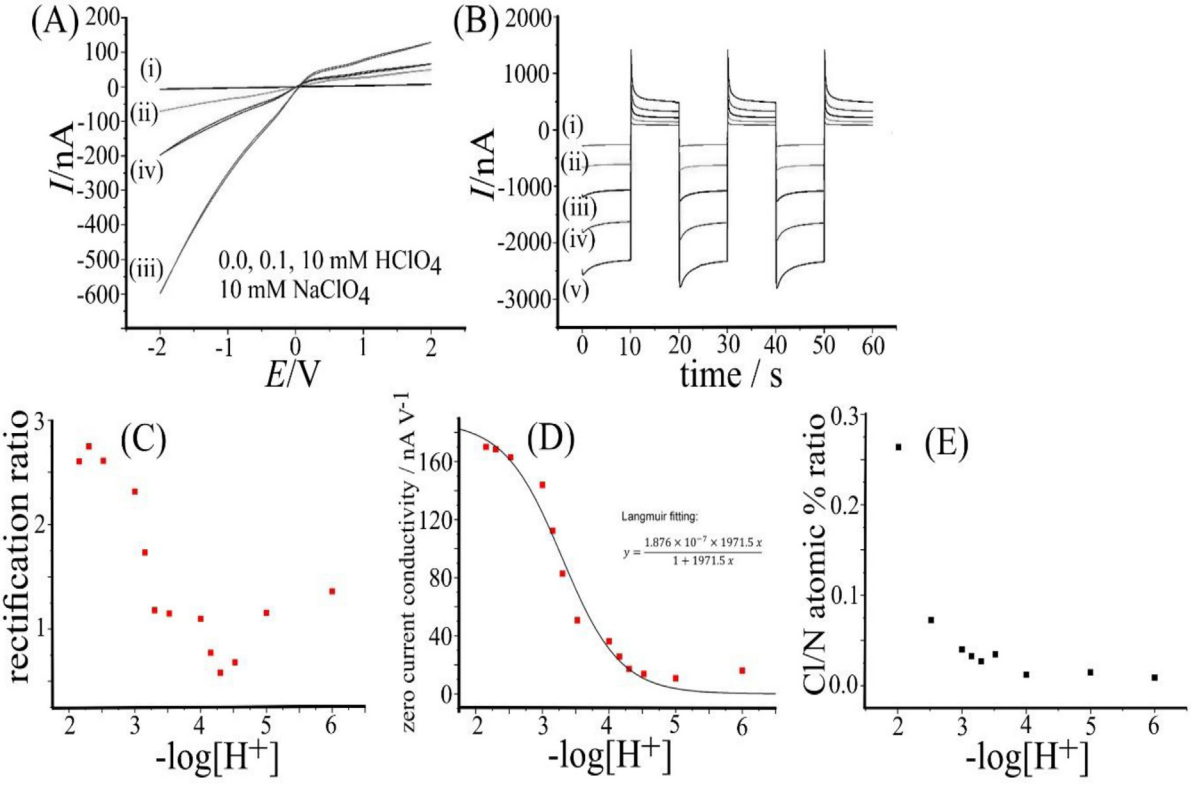

Fig. 8. (A) Cyclic voltammograms (four-electrode configuration, scan rate 0.2 V s^{-1}) for PIM-EA-TB on a 10 μm diameter microhole substrate in 10 mM $NaClO_4$ in ethanol with (i) 0.0, (ii) 0.1, (iii) 10 mM $HClO_4$. In (iv) the PIM-EA-TB was returned from 10 to 0 mM $HClO_4$ and left over night. (B) chronoamperometry data for 10 mM $NaClO_4$ with 10 mM $HClO_4$ in ethanol with (i) 1, (ii) 2, (iii) 3, (iv) 4, and (v) 5 V potential steps. (C) Rectification ratio data from chronoamperometry at +/- 1 V. (D) Langmuir plot for zero current conductivity versus logarithm of proton concentration. (E) Plot of Cl/N atomic ratio from EDX data versus logarithm of proton concentration.

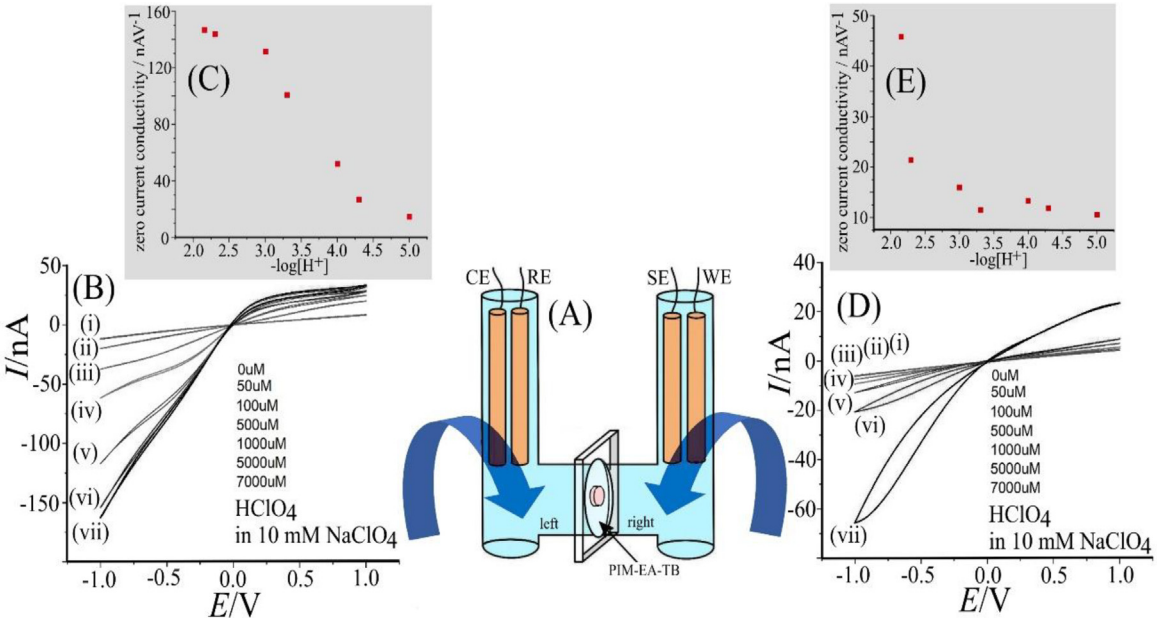

Fig. 9. (A) Illustration of left and right compartments for addition of $HClO_4$. (B) Cyclic voltammograms (four-electrode configuration, scan rate 0.2 V s^{-1}) for PIM-EA-TB on a 10 mm diameter microhole substrate in 10 mM $NaClO_4$ in ethanol with addition to the counter electrode side of (i) 0.0, (ii) 0.05, (iii) 0.1, (iv) 0.5, (v) 1, (vi) 5, (vii) 7 mM $HClO_4$. (C) Zero current conductivity plot as a function of proton concentration. (D) As before, but acid addition to the working electrode side. (E) Zero current conductivity plot as a function of proton concentration.

Table 2
EDX data (atomic %) for PIM-EA-TB films on Teflon exposed (15 min) to 10 mM $NaClO_4$ containing $HClO_4$ and rinsed with ethanol prior to analysis.

log[H^+]	EDX map sum spectrum: Atomic %					Cl/N ratio
	C	N	O	F	Cl	
−2	76.5	8.9	11.8	0.39	2.34	0.263
−2.52	84	10.1	4.61	0.56	0.73	0.073
−3	85.8	9.71	3.86	0.13	0.39	0.040
−3.52	88.5	8.38	2.38	0.42	0.29	0.035
−3.3	85.1	11.2	2.8	0.6	0.3	0.027
−3.15	87.3	8.56	3.42	0.37	0.28	0.033
−4	86.5	9.95	2.82	0.53	0.12	0.012
−5	86.4	8.14	3.62	1.59	0.12	0.015
−6	89.6	8.98	1.08	0.21	0.08	0.009

ionic diode effects are observed with a “half protonation point” at approx. 0.3 mM $HClO_4$ (which is not dissimilar to the value in Fig. 8D). Protonation of the PIM-EA-TB directly in the microhole region (counter electrode side) appears to be more effective when compared to protonation of the PIM-EA-TB from the opposite (working electrode) side.

The effect of protons is highest in the counter electrode compartment. Therefore, a platinum electrode can be employed (using a second working electrode and a bipotentiostat) to produce protons locally at the location of the PIM-EA-TB membrane in this compartment. Fig. 10B illustrates the experimental approach with a platinum electrode approx. 0.5 mm away from the PIM-EA-TB film. Fig. 10A shows cyclic voltammetry data for (i) the initial state of the film in 10 mM $NaClO_4$ in ethanol. After applying a 1.75 V vs Ag fixed bias voltage to the secondary working electrode over a period of 400 s (an anodic current of 60 μA is observed; during 10 potential cycles employing the cyclic voltammetry mode) protons are generated and the cyclic voltammogram changes to that of an ionic diode (Fig. 10Aii). The diode state persists with the secondary working electrode turned off. Only when a negative bias is applied to the platinum electrode (400 s at −1.75 V vs Ag; cathodic current −10 μA) can the PIM-EA-TB film be reverted to the insulating state (Fig. 10Aiii).

Chronoamperometry data confirm the protonation and deprotonation due to electrochemical gating. Fig. 10C shows chronoamperometry results for the initial state (i), the protonated state (ii), and the deprotonated state (iii). Impedance methods can be employed to characterise the behaviour of the PIM-EA-TB film with/without protonation. Fig. 10D shows typical Nyquist plots for PIM-EA-TB immersed in 10 mM $NaClO_4$ in ethanol. A 4-electrode configuration is employed and the semicircle represents the capacitance of the Teflon film (typically 0.6 nF; at high frequency conductivity due to the capacitor prevails; data summarised in Table 3) with a series resistance due to the electrolyte solution and contacts (R1). The parallel resistance R2 is associated with the microhole region conductivity and with the PIM-EA-TB film deposit (R2, dominated by the PIM-EA-TB and the microhole region in the Teflon [33]).

Dataset (i) describes the initial state of the PIM-EA-TB film. When protons are generated at the secondary working electrode, protonation of the PIM-EA-TB occurs, and the conductivity increases. In dataset (ii) the value for R2 changes by an order of magnitude. In dataset (iii) the deprotonation can be seen to revert the value for R2 to less conductive.

For the case of the protonated state, a further low frequency “tail” is produced due to the ionic diode switching between open and closed states. There are several time constants associated with (i) the

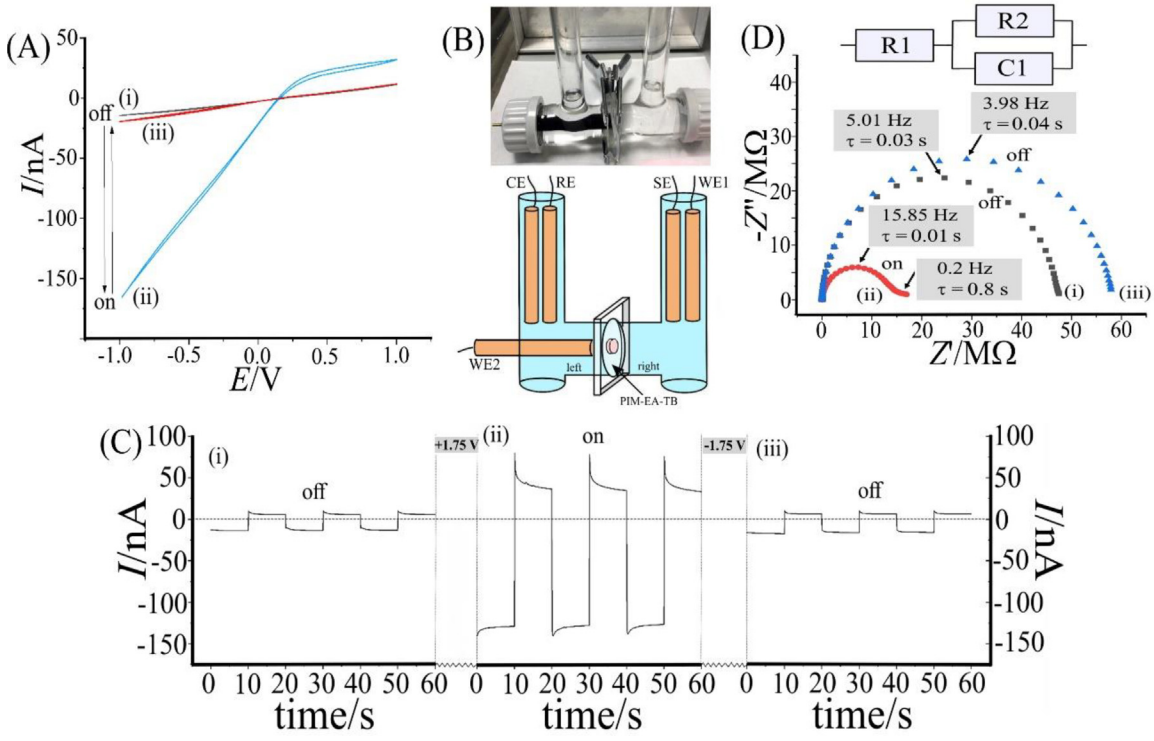

Fig. 10. (A) Cyclic voltammograms (four-electrode configuration, scan rate 0.2 V s^{-1}) for PIM-EA-TB on a 10 μm diameter microhole substrate in 10 mM $NaClO_4$ in ethanol with a 3 mm diameter Pt electrode placed into the counter electrode compartment: (i) initial voltammogram; (ii) after 400 s 1.75 V vs Ag fixed applied potential to switch to the on state; (iii) after 400 s −1.75 V vs Ag fixed applied to switch the diode back to the off state. (B) Illustration and photograph of the experiment. (C) Chronoamperometry data (−1/+1 V vs Ag) going from (i) initial state to (ii) on state (180 s 1.75 V vs Ag) and (iii) to off state (180 s −1.75 V vs Ag). (D) Impedance spectroscopy data (frequency range from 100 KHz to 0.1 Hz; bias potential 0.0 V vs Ag; amplitude 0.1 V; Nyquist plots) going from (i) initial state to (ii) on state (180 s 1.75 V vs Ag) and (iii) to off state (180 s −1.75 V vs Ag). Semicircle summit frequencies and time constants $\tau = (2\pi f)^{-1}$ indicated.

Table 3
Summary of impedance data (frequency range from 100 KHz to 0.1 Hz; bias potential 0.0 V vs Ag; amplitude 0.1 V) going from (i) initial state to (ii) on state (180 s 1.75 V vs Ag) and (iii) to off state (180 s −1.75 V vs Ag). The semicircular feature was fitted with an $R_1[R_2C1]$ circuit (fitting errors in brackets). The time constant for ion transport was obtained from τ = R2 × C1.

	R1/KΩ	C1/nF	R2/MΩ	τ/s
(i) OFF	9.5 (<3%)	0.59 (<2%)	46.1 (<2%)	0.028
(ii) ON	9.3 (<4%)	0.56 (<2%)	12.3 (<3%)	0.008
(iii) OFF	10.2 (<3%)	0.56 (<2%)	54.9 (<3%)	0.033

charging of the Teflon film via R1 (typically 10 microseconds), (ii) the onset of ion flow through the microhole (typically 0.01 s), and (iii) the switching of the diode state between open and closed states (typically 0.8 s). The much slower diode switching time constant is in agreement with chronoamperometry data (Fig. 10C) and with literature values [31]. Physically, the switching time is associated with the migration-diffusion of anions and cations into/out of the microhole space (see Fig. 1B).

4. Conclusions

Ionic diode behaviour has been demonstrated for PIM-EA-TB as a microporous polyamine immersed in ethanol solutions of various perchlorate salts. In contrast to similar processes in aqueous media, the background level ion transport for 10 mM $NaClO_4$ through the neutral PIM-EA-TB film remains very low (probably due to better ion/size exclusion in ethanol) even with applied voltages. Only when charges are attached to the polymer via protonation of the tertiary amine sites, anion transport and improved conductivity are observed.

The asymmetrically deposited film of PIM-EA-TB on a Teflon film with 10 μm diameter microhole allows ionic diode/rectification behaviour to be observed. An anionic diode is observed due to predominant anion transport in the protonated film. When exploring reactivity of a range of cations, Cu^{2+} stands out as being able to trigger anionic diode behaviour. This has been shown to be linked to formation of acidic protons and protonation of PIM-EA-TB rather than due a direct interaction of Cu^{2+} with the polymer.

Switching of the diode state was demonstrated not only by adding acid, but also by locally generating acid/base with a platinum electrode placed in the vicinity of the PIM-EA-TB polymer film. In the future, this kind of electrochemical gating (when miniaturised) could be employed in ionic circuits to switch diode behaviour and to control the transport of ions and of neutral species (in rectified electroosmosis).

CRediT authorship contribution statement

Zhongkai Li: Conceptualization, Data curation, Formal analysis, Writing - original draft. **Philip J. Fletcher:** . **Mariolino Carta:** Supervision, Conceptualization, Writing - review & editing. **Neil B. McKeown:** Supervision, Conceptualization, Writing - review & editing. **Frank Marken:** Supervision, Conceptualization, Formal analysis, Methodology, Resources, Writing - review & editing.

Data availability

No data was used for the research described in the article.

Declaration of Competing Interest

The authors declare that they have no known competing financial interests or personal relationships that could have appeared to influence the work reported in this paper.

Acknowledgements

F.M. thanks for the initial financial support by the EPSRC (EP/K004956/1).

References

[1] X. Hou, W. Guo, L. Jiang, Biomimetic smart nanopores and nanochannels, Chem. Soc. Rev. 40 (5) (2011) 2385–2401.
[2] H.S. White, A. Bund, Ion current rectification at nanopores in glass membranes, Langmuir 24 (5) (2008) 2212–2218.
[3] Z.S. Siwy, S. Howorka, Engineered voltage-responsive nanopores, Chem. Soc. Rev. 39 (3) (2010) 1115–1132.
[4] L.J. Cheng, L.J. Guo, Review nanopores Nanofluidic diodes, Chem. Soc. Rev. 39 (3) (2010) 923–938.
[5] B.R. Putra, L. Tshwenya, M.A. Buckingham, J.Y. Chen, K.J. Aoki, K. Mathwig, O.A. Arotiba, A.K. Thompson, Z.K. Li, F. Marken, Microscale ionic diodes: an overview, Electroanalysis 33 (6) (2021) 1398–1418.
[6] W.J. Lan, M.A. Edwards, L. Luo, R.T. Perera, X.J. Wu, C.R. Martin, H.S. White, Voltage-rectified current and fluid flow in conical nanopores, Acc. Chem. Res. 49 (11) (2016) 2605–2613.
[7] Z.K. Li, R. Malpass-Evans, N.B. McKeown, M. Carta, K. Mathwig, J.P. Lowe, F. Marken, Effective electroosmotic transport of water in an intrinsically microporous polyamine (PIM-EA-TB), Electrochem. Commun. 130 (2021) 107110.
[8] Z.K. Li, L.N. Wang, R. Malpass-Evans, M. Carta, N.B. McKeown, K. Mathwig, P.J. Fletcher, F. Marken, Ionic diode and molecular pump phenomena associated with caffeic acid accumulated into an intrinsically microporous polyamine (PIM-EA-TB), ChemElectroChem 8 (11) (2021) 2044–2051.
[9] E. Madrid, P. Cottis, Y.Y. Rong, A.T. Rogers, J.M. Stone, R. Malpass-Evans, M. Carta, N.B. McKeown, F. Marken, Water desalination concept using an ionic rectifier based on a polymer of intrinsic microporosity (PIM), J. Mater. Chem. A 3 (31) (2015) 15849–15853.
[10] B.R. Putra, E. Madrid, L. Tshwenya, O.A. Arotiba, F. Marken, An AC-driven desalination/salination system based on a Nafion cationic rectifier, Desalination 480 (2020) 114351.
[11] X.D. Huang, X.Y. Kong, L.P. Wen, L. Jiang, Review nanopores bioinspired ionic diodes: from unipolar to bipolar, Adv. Functional Mater. 28 (49) (2018) 1801079.
[12] I. Boussouar, Q.J. Chen, X. Chen, Y.L. Zhang, F. Zhang, D.M. Tian, H.S. White, H.B. Li, Single nanochannel platform for detecting chiral drugs, Anal. Chem. 89 (2) (2017) 1110–1116.
[13] J. Wang, Y.H. Zhou, L. Jiang, Bio-inspired track-etched polymeric nanochannels: steady-state biosensors for detection of analytes, ACS Nano 15 (12) (2021) 18974–19013.
[14] F. Marken, L.N. Wang, Y.Z. Zhao, Z.K. Li, M. Amiri, H. Imanzadeh, Polymers of intrinsic microporosity (PIMs) in sensing and in electroanalysis, Curr. Opinion Chem. Engineer. 35 (2022) 100765.
[15] S. Bearden, E. Simpanen, G. Zhang, Active current gating in electrically biased conical nanopores, Nanotechnology 26 (18) (2015) 185502.
[16] Q. Liu, K. Xiao, L.P. Wen, H. Lu, Y.H. Liu, X.Y. Kong, G.H. Xie, Z. Zhang, Z.S. Bo, L. Jiang, Engineered ionic gates for ion conduction based on sodium and potassium activated nanochannels, J. Amer. Chem. Soc. 137 (37) (2015) 11976–11983.
[17] S. Nasir, M. Ali, P. Ramirez, K. Froehlich, J. Cervera, S. Mafe, W. Ensinger, Ionic conduction through single-pore and multipore polymer membranes in aprotic organic electrolytes, J. Mem. Sci. 635 (2021) 119505.
[18] Y.Y. Rong, Q.L. Song, K. Mathwig, E. Madrid, D.P. He, R.G. Niemann, P.J. Cameron, S.E.C. Dale, S. Bending, M. Carta, R. Malpass-Evans, N.B. McKeown, F. Marken, pH- induced reversal of ionic diode polarity in 300 nm thin membranes based on a polymer of intrinsic microporosity, Electrochem. Commun. 69 (2016) 41–45.
[19] N.B. McKeown, P.M. Budd, Exploitation of intrinsic microporosity in polymer-based materials, Macromolecules 43 (12) (2010) 5163–5176.
[20] P.M. Budd, B.S. Ghanem, S. Makhseed, N.B. McKeown, K.J. Msayib, C.E. Tattershall, Polymers of intrinsic microporosity (PIMs): robust, solution-processable, organic nanoporous materials, Chem. Commun. 2 (2004) 230–231.
[21] M. Carta, R. Malpass-Evans, M. Croad, Y. Rogan, J.C. Jansen, P. Bernardo, F. Bazzarelli, N.B. McKeown, An efficient polymer molecular sieve for membrane gas separations, Science 339 (6117) (2013) 303–307.
[22] E. Madrid, Y.Y. Rong, M. Carta, N.B. McKeown, R. Malpass-Evans, G.A. Attard, T.J. Clarke, S.H. Taylor, Y.T. Long, F. Marken, Metastable ionic diodes derived from an amine-based polymer of intrinsic microporosity, Angew. Chem. Inter. Ed. 53 (40) (2014) 10751–10754.
[23] Y.Y. Rong, A. Kolodziej, E. Madrid, M. Carta, R. Malpass-Evans, N.B. McKeown, F. Marken, Polymers of intrinsic microporosity in electrochemistry: anion uptake and transport effects in thin film electrodes and in free-standing ionic diode membranes, J. Electroanal. Chem. 779 (2016) 241–249.
[24] K. Mathwig, B.D.B. Aaronson, F. Marken, Ionic transport in microhole fluidic diodes based on asymmetric ionomer film deposits, ChemElectroChem 5 (6) (2018) 897–901.
[25] T.L. Frey, K.R. Fruehauf, R.A. Lucas, J.W. Polster, K.J. Shea, Z.S. Siwy, Electrochemical probing of steric, electrostatic and hydrophobic interactions of large cations in polymers of intrinsic microporosity, J. Electrochem. Soc. 169 (2) (2022) 020566.
[26] N.B. McKeown, P.M. Budd, Polymers of intrinsic microporosity (PIMs): organic materials for membrane separations, heterogeneous catalysis and hydrogen storage, Chem. Soc. Rev. 35 (8) (2006) 675–683.
[27] M. Gigli, J.A. Kowalski, B.J. Neyhouse, A. D'Epifanio, F.R. Brushett, S. Licoccia, Investigating the factors that influence resistance rise of PIM-1 membranes in nonaqueous electrolytes, Electrochem. Commun. 107 (2019) 106530.
[28] S.E. Doris, A.L. Ward, A. Baskin, P.D. Frischmann, N. Gavvalapalli, E. Chenard, C.S. Sevov, D. Prendergast, J.S. Moore, B.A. Helms, Macromolecular design strategies for preventing active-material crossover in non-aqueous all-organic redox-flow batteries, Angew. Chem. Inter. Ed. 56 (6) (2017) 1595–1599.
[29] B.R. Putra, M. Carta, R. Malpass-Evans, N.B. McKeown, F. Marken, Potassium cation induced ionic diode blocking for a polymer of intrinsic microporosity | nafion “heterojunction” on a microhole substrate, Electrochim. Acta 258 (2017) 807–813.
[30] Y. Marcus, Ion Properties, Marcel Dekker, New York, 1997.
[31] D.P. He, E. Madrid, B.D.B. Aaronson, L. Fan, J. Doughty, K. Mathwig, A.M. Bond, N.B. McKeown, F. Marken, A cationic diode based on asymmetric nafion film deposits, ACS Appl. Mater. Interfaces 9 (12) (2017) 11272–11278.
[32] B.R. Putra, K. Szot-Karpinska, P. Kudla, H. Yin, J.A. Boswell, A.M. Squires, M.A. Da Silva, K.J. Edler, P.J. Fletcher, S.C. Parker, F. Marken, Bacteriophage M13 aggregation on a microhole poly(ethylene terephthalate) substrate produces an anionic current rectifier: sensitivity toward anionic versus cationic guests, ACS Appl. Bio Mater. 3 (1) (2020) 512–521.
[33] Z.K. Li, T. Pang, J. Shen, P.J. Fletcher, K. Mathwig, F. Marken, Ionic diode desalination: combining cationic Nafion™ and anionic Sustainion™ rectifiers, Micro Nano Engineer. 16 (2022) 100157.